Mechanical alloying: a pressure induced reaction for obtaining zinc blende GaSb and multiphase states

2006 J. Phys.: Condens. Matter 18 8613

(http://iopscience.iop.org/0953-8984/18/37/019)

INSTITUTE OF PHYSICS PUBLISHING JOURNAL OF PHYSICS: CONDENSED MATTER

J. Phys.: Condens. Matter **18** (2006) 8613–8622 doi:10.1088/0953-8984/18/37/019

Mechanical alloying: a pressure induced reaction for obtaining zinc blende GaSb and multiphase states

C E M Campos[1,4], J C de Lima[1], T A Grandi[1], M Schmitt[2] and P S Pizani[3]

[1] Departamento de Física, Universidade Federal de Santa Catarina, CP 476, 88040-900 Florianópolis, SC, Brazil
[2] Departamento de Engenharia Mecânica, Universidade Federal de Santa Catarina, CP 476, 88040-900 Florianópolis, SC, Brazil
[3] Departamento de Física, Universidade Federal de São Carlos, CP 676, 13 565-905 São Carlos, SP, Brazil

E-mail: pcemc@fisica.ufsc.br

Received 30 March 2006, in final form 24 July 2006
Published 1 September 2006
Online at stacks.iop.org/JPhysCM/18/8613

Abstract

The cubic zinc blende GaSb phase was produced by a mechanical alloying technique, which is a solid state route based on the action of non-hydrostatic pressures. The thermal stability of this phase was tested using the differential scanning calorimetry technique and, in order to clarify the results, an annealing process was performed. Comparing x-ray diffraction patterns for as-prepared and annealed samples, the improvement in crystallinity of the cubic phase and Sb segregation and/or crystallization can be easily seen. Optical phonons frequencies were measured for both as-milled and annealed samples by means of the Raman spectroscopy technique. Raman profiles of as-milled samples showed typical zinc blende GaSb optical modes and revealed new features that can be associated with multiphase states.

1. Introduction

The advent of nanostructured materials has made it possible to imagine a wide range of new developments with technological applications, since new solids with desired properties can be designed. This is associated with the presence of the atomic arrangements located at defect centres, such as grain boundaries and interphase boundaries, allowing one to produce solids with new atomic structures and physical properties.

Mechanical alloying (MA) has been used as a technique for synthesizing amorphous, crystalline phases and solid solutions as well as nanostructured materials [1–4]. MA has permitted the production of powders in bulk form, facilitating the fabrication of massive pieces via consolidation [5].

[4] Author to whom any correspondence should be addressed.

From the experimental point of view, MA is a dry milling process in which blended crystalline elemental metal and/or non-metal powders are actively deformed by non-hydrostatic pressures in a controlled atmosphere, under a highly energetic ball charge. In the first stage of milling the main effect is a fast reduction of particle size of the mixture components and, after a short period of milling, the powder particles are cold welded by the colliding balls, resulting in composite powder particles that show a layered microstructure with a preferred orientation. The fast reduction of particle size of the mixture components into smaller crystallites down to nanometre size also produces an interfacial component made of defect centres (grain boundaries, interphase boundaries, dislocations, etc). Further milling leads to ultrafine composite powder particles where solid state reactions take place. Thus, from the structural point of view, nanometre powders must be analysed in terms of two components, one crystalline, that preserves the structure of bulk crystal, and another interfacial, composed of defect centres.

Although the usual way to pressure induce phase transitions is through hydrostatic conditions obtainable with diamond anvil cells (DAC), non-hydrostatic pressure conditions can result in very interesting phase transitions. For instance, a theoretically predicted InSb wurtzite phase [6, 7] was just confirmed by indentation which is a process based on hugely non-hydrostatic conditions [8, 9]. Furthermore, recently Pizani *et al* [10] have studied the effects of applying high non-hydrostatic pressures to InSb, GaSb and GaAs by mechanical impact. They observed small, micrometre regions with wurtzite structure corroborating the theoretical predictions for InSb and GaAs. For GaSb, although not predicted theoretically, a similar behaviour was reported.

The Ga–Sb system has attracted the attention of many researchers as a potential candidate for high speed, low power electronic device use [11] and because of its potential application in semiconductor mid-infrared lasers with emission wavelengths in the range of 2–4 μm. These devices are promising for a variety of military and civil applications such as in low noise, high frequency amplifiers, infrared imaging sensors, fire detection and for monitoring environmental pollution [12]. The phase diagram [13] exhibits a single equiatomic compound, which in accordance with the JCPDS Database [14] can occur in the cubic, tetragonal, hexagonal and orthorhombic structures. This compound has been produced by several techniques such as sputtering [15], quenching [16], SAMP [17], solid source molecular beam epitaxy [12] and liquid phase epitaxy [18]. Recently, some authors [19] have studied the effects of ball milling on Sb and Ga–Sb systems in air atmosphere. They observed that the antimony metal was oxidized and formed the high temperature orthorhombic Sb_2O_3 phase, and estimated the temperature of the milling as being as high as 570 °C.

In this paper we describe the formation of a cubic GaSb phase (zinc blende type) by MA, which provides non-hydrostatic pressure conditions, and the results for its structural, thermal and optical properties obtained through XRD, differential scanning calorimetry (DSC) and Raman spectroscopy measurements.

2. Experimental procedure

An equiatomic mixture of high purity elemental Ga (Aldrich 99.999%) and Sb powder (Alfa Aesar 99.999%, −200 mesh) was sealed together with seven steel balls 11.0 mm in diameter into a cylindrical steel vial (diameter 40 mm and length 55 mm) under an argon atmosphere. The ball-to-powder weight ratio was 5:1. A Spex Mixer/mill, model 8000 (working with 1425 rpm), was then used to perform MA at room temperature. After 2 and 9 h of milling, the process was stopped and the as-milled powder was analysed by XRD and microanalysis techniques. The microanalysis results reveal a slight deviation of equiatomic composition

(54 at.% Ga). We have also investigated other mixtures of Ga and Sb by MA. For those rich in Ga, almost all gallium content remained glued to the internal wall of the steel vial after few hours of milling. For those rich in Sb, the measured XRD patterns exhibited the cubic GaSb phase together with the rhombohedral Sb one. Some results for one of the Sb-rich mixtures, $Ga_{30}Sb_{70}$, are also described in this paper when appropriate. All the XRD patterns were recorded using a Philips Xpert powder diffractometer with Cu Kα radiation ($\lambda = 0.154\,06$ nm).

The thermal analyses were performed using the DSC technique. The DSC spectrum was recorded from 20 to 600 °C, with a heating rate of 10 °C min^{-1}, under flowing nitrogen in a 2010 DSC cell manufactured by TA Instruments. All enthalpy measurements are given in joules per gram (J g^{-1}), of the entire sample weight. In order to clarify the DSC results, an amount of as-milled sample was sealed in a quartz tube evacuated to about 10^{-3} Torr, and annealed at 600 °C for 150 min; this was followed by air cooling.

Micro-Raman measurements were performed with a T64000 Jobin–Yvon triple monochromator coupled to an optical microscope, a cooled CCD detector and a conventional photon counting system. The 5145 Å line of an argon ion laser was used as the exciting light, always in backscattering geometry. The output power of the laser was kept under 800 μW to avoid overheating the samples. The laser beam focused on the sample surface using a 100× objective results in a spot probe of about 1 μm square. All measurements were performed at room temperature. Two spectra were collected from visibly different parts of the surface of both samples, which were named regions #1 and #2. The regions #1 were identified by the optical microscope as flat in shape and having light colorations. This is the predominant surface appearance. The regions #2 were associated with clusters and islands with irregular shapes and with dark and/or bright aspects that are immersed in the predominant region (#1).

3. Results and discussion

3.1. X-ray diffraction and differential scanning calorimetry measurements

Figure 1 shows x-ray diffraction patterns for $Ga_{50}Sb_{50}$ and $Ga_{30}Sb_{70}$ nominal mixtures milled up to 9 and 8 h, respectively. From this figure one can see that for the $Ga_{50}Sb_{50}$ mixture the solid state reaction takes place after just 2 h of milling, which is also seen for Sb-rich mixture where the Sb excess can be observed in its crystalline form (see the symbols in figure 1).

The XRD pattern for the $Ga_{50}Sb_{50}$ sample milled for 9 h was compared with all the GaSb ones given in the JCPDS Database [14] and it was found to agree with the cubic phase (card No 07-0215). Then, it was fitted considering a single GaSb cubic phase using the Rietveld refinement structure procedure [20] with a pseudo-Voigt function type through the DBWS 9807 code. For that, the crystallographic data (lattice parameter, space group, atomic positions, etc) for the cubic GaSb phase (ZnS sphalerite prototype) were taken from the TAPP 2.2 software [21], and the best fit was reached by considering the lattice parameter $a = 0.6086$ nm. The TAPP 2.2 software and the JCPDS Database give $a = 0.609\,59$ and 0.6095 nm, respectively. The fitted pattern is shown in figure 2 where one can observe excellent agreement between it and the experimental one.

As the experimental XRD pattern showed all peaks broadened, indicating (according to the Williamson–Hall approach [22]) a strained nanometre structure, the mean crystallite size of the as-milled sample was estimated from the XRD fitting results. This takes into account effects of line broadening caused by both crystallite size and strain through the relationship [23]

$$\left(\frac{\beta_t \cos\theta}{K\lambda}\right)^2 = \frac{1}{d^2} + \sigma_p^2\left(\frac{\sin\theta}{K\lambda}\right)^2, \tag{1}$$

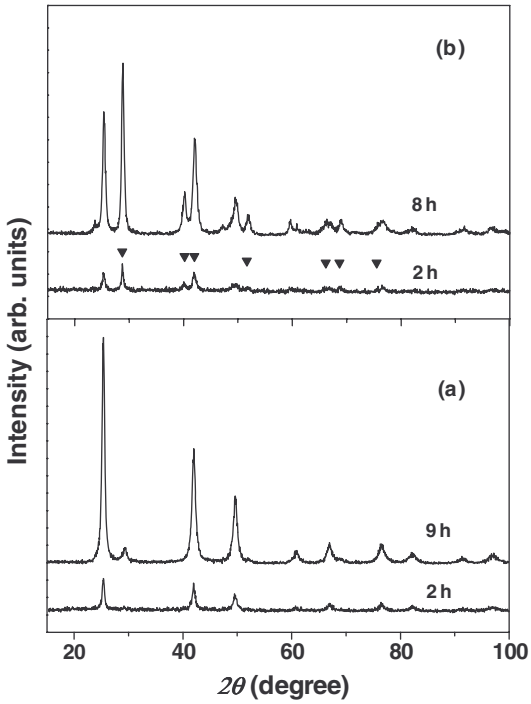

Figure 1. X-ray diffraction patterns for as-milled $Ga_{50}Sb_{50}$ (a) and $Ga_{30}Sb_{70}$ (b) mixtures. Down triangles show the rhombohedral Sb main peaks positions.

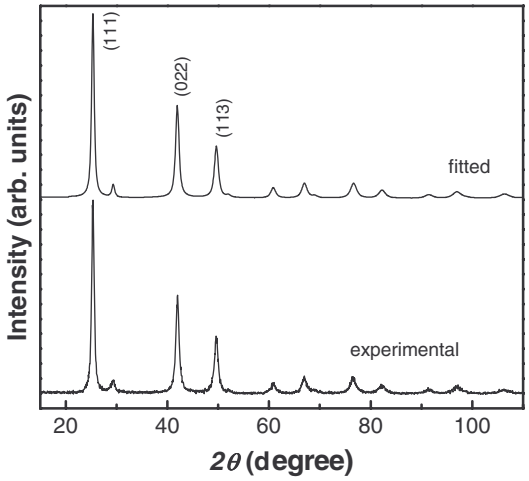

Figure 2. Experimental and fitted x-ray diffraction patterns for $Ga_{50}Sb_{50}$ milled for 9 h.

where θ is the diffraction angle, λ is the x-ray wavelength, β_t is the total broadening measured at the peak's full width at half-maximum (FWHM) in radians, d is the crystal size, σ_p is the strain, and K is the Scherrer constant (assumed as 0.91) and for the units of β_t and d. Graphical regression of the relationship (1), i.e. plotting of $\beta_t^2 \cos^2\theta/\lambda^2$ versus $\sin^2\theta/\lambda^2$, yields the mean crystal size (free of strain effects) and the strain from the values of the intercept of the straight

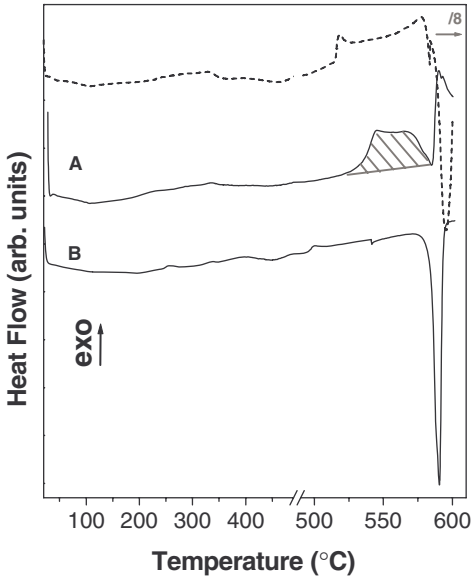

Figure 3. DSC curves for as-milled (A) and annealed (B) $Ga_{50}Sb_{50}$ samples. The dashed (thin) line shows the DSC curve for the $Ga_{30}Sb_{70}$ sample.

regression line obtained and from its slope, respectively. The values obtained for the as-milled $Ga_{50}Sb_{50}$ sample were $d \approx 13$ nm and $\sigma_p \approx 3.0\%$.

Figure 3 shows DSC curves for as-milled $Ga_{50}Sb_{50}$ (labelled A) and $Ga_{30}Sb_{70}$ (dashed line) samples. From the DSC curve for the as-milled $Ga_{50}Sb_{50}$ sample (curve A) one can see a broad exothermic band located between 100 and 450 °C and a sharp exothermic peak located at about 550 °C, which seems to be composed by two peaks. The enthalpy change was calculated by integrating the area under the sharp peak (illustrated in figure 3), and the value found was 13.5 J g^{-1}. This feature is very similar to that observed for the amorphous–crystalline phase transition of Ga–Sb near the equiatomic composition, whose mean value for the integral exothermic heat reported was 3.5 KJ mol^{-1} (18.3 J g^{-1}) [24]. However, in this study the temperature range is noticeably different from that presented in [24] (130 and 350 °C), but it is very important to notice that sample preparation paths are completely dissimilar, which can be pointed out as the main reason for such different temperature ranges.

The DSC curve for the as-milled $Ga_{30}Sb_{70}$ sample (dashed line) also shows a broad exothermic band located between 100 and 450 °C and some sharp exothermic features at about 510 and 560 °C that are follow by a strong endothermic reaction at about 590 °C. The sharp exothermic feature is indicative of a Ga–Sb amorphous phase and the endothermic reaction is attributed to the rhombohedral Sb melting, which appears approximately 35 °C below the bulk rhombohedral Sb melting point (631 °C), as predicted for dilute solid solutions containing about 10 at.% Ga, shown in the phase diagram [21]. The enthalpy change due to Sb melting in the $Ga_{30}Sb_{70}$ sample was partially estimated (since the peak is incomplete due to limitations of Al pans used in the DSC cell) as 59.0 J g^{-1}.

In order to clarify the exothermic reactions for the as-milled $Ga_{50}Sb_{50}$ sample, it was annealed at 600 °C for 150 min. The XRD pattern of the annealed sample is shown in figure 4 (the noisy pattern at the bottom). A comparison between figures 4 and 2 shows that there was no crystalline phase transformation, and all diffraction peaks became sharper and more intense than before annealing, indicating an improvement in the crystallinity of the annealed sample.

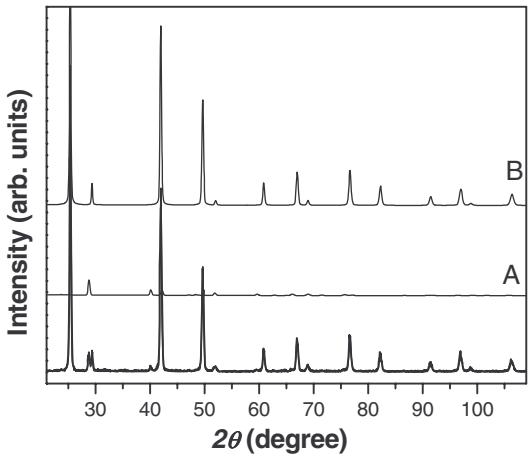

Figure 4. Experimental and simulated x-ray diffraction patterns for annealed $Ga_{50}Sb_{50}$ sample. Curves B and A show the contributions of cubic GaSb and rhombohedral Sb phases to the total simulated pattern, respectively.

Thus, exothermic broad band seen in the DSC curves was attributed to the structural relaxation: elimination of stress, strain, point and line defects, and grain growth processes. The XRD pattern of the annealed sample also showed rhombohedral Sb diffraction peaks (ICSD [25] code No 9859), which is in total agreement with the DSC curve for the annealed sample (see curve B in figure 3) which shows Sb melting at about 590 °C with an enthalpy change of 13.2 J g^{-1}.

The V element migration in III–V semiconductors is a well known effect [26, 27] and can be liable to having Sb diffraction peaks appearing in XRD pattern. However, the coalescence of antimony particles could be originating from very small particles, or even atoms, dispersed in the interfacial component of the as-milled powder, which were not detected in the XRD pattern and in the DSC spectrum, due to the well dispersed condition (not forming a rhombohedral lattice).

We have also fitted the measured XRD pattern for the annealed $Ga_{50}Sb_{50}$ sample. Besides the cubic GaSb phase, the rhombohedral Sb phase was taken into account. The fitted pattern is shown in figure 4 (overlapped with experimental one). In this figure the contributions of rhombohedral Sb and cubic GaSb phases to the total fitted pattern are also shown separately (see curves A and B, respectively). The best fitting was reached by considering the lattice parameter $a = 0.6084$ nm for the GaSb phase and $a = 0.4281$ nm and $c = 1.1281$ nm for the Sb one. The JCPDS card gives $a = 0.4300$ nm and $c = 1.1222$ for Sb. The DBWS 9807 code was used to calculate the relative amounts of crystalline phases, and the values obtained were 95% and 5% for GaSb and Sb, respectively.

The mean crystallite size and strain for annealed $Ga_{50}Sb_{50}$ sample were also calculated from the fitting XRD results and equation (1). The values found were $d \approx 26$ nm and $\sigma_p \approx 0.90\%$. The increasing of the mean crystallite size due to annealing can be associated with the reduction of the interfacial component. The changes observed in the XRD pattern for the annealed sample are associated with the improvement of crystallinity, increase in mean crystallite size and reduction of strains.

3.2. Raman measurements

The Raman spectrum of the as-milled and annealed $Ga_{50}Sb_{50}$ samples depends essentially on the region of the surface where the measurement was performed. Over most of that surface

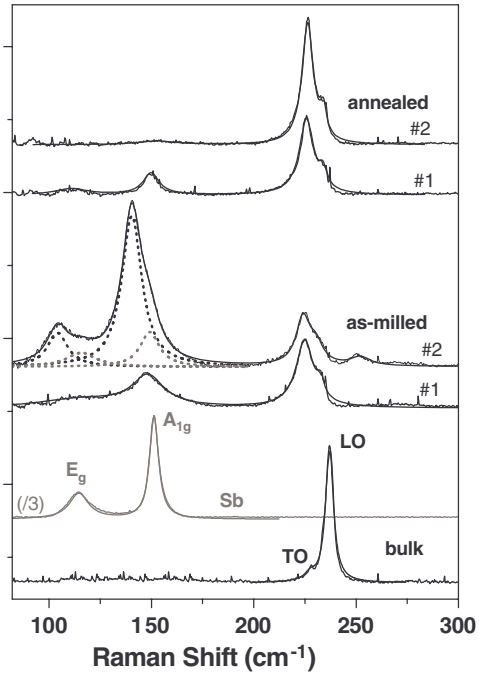

Figure 5. Raman spectra for bulk GaSb, as-milled and annealed $Ga_{50}Sb_{50}$ samples. The grey line shows the spectrum of rhombohedral Sb bulk sample.

Table 1. Raman line positions resulting from the spectra fitting using Lorentzian functions.

		1	2	3	4	5	6	7
GaSb bulk						227.6	237.0	
Sb			114.6		151.3			
As-milled	#1		115.9		148.3	224.9	232.7	
GaSb	#2	104.1	115.7	140.4	149.2	224.0	230.3	252.2
Annealed	#1		111.0		149.8	225.8	233.9	
GaSb	#2				148.2	226.3	234.0	

parts of the as-milled and annealed $Ga_{50}Sb_{50}$ samples well known spectra were found, with peaks due to the zinc blende structure. Figure 5 shows the Raman spectra for as-milled and annealed $Ga_{50}Sb_{50}$ samples and, for refere nce, the Raman spectra of bulk GaSb and Sb. All the spectra were fitted using Lorentzian functions and the frequency values obtained are listed in table 1.

From this figure one can see two spectra, collected from visibly different parts of the surface (marked as #1 and #2), for each (as-milled and annealed) sample, where it is possible to identify the longitudinal and transverse optical phonons (LO and TO, respectively) of zinc blende GaSb phase. Moreover, in all spectra one can see features in the low frequency range (<170 cm^{-1}). These features correspond to the same spectral region of A_{1g} and E_g optical modes of rhombohedral Sb. However, critical assessment must be done before assuming that the low frequency features of as-milled and annealed $Ga_{50}Sb_{50}$ spectra are just due to Sb optical phonons:

(i) The A_{1g}/TO line intensity ratio observed in one of the spectra (#2) for the as-milled sample reached huge values (>3.00) that suggest a large amount of crystalline Sb in this sample, which is in total contradiction with the XRD and DSC results. Repeated measurements on different positions of this sample reproduced the low frequency modes (see spectrum #1), although they showed important frequency shifts and intensity reduction, suggesting Sb-poor regions. Then, several reasons can be pointed out to explain this discrepancy. One of them is that there were different sample sensitivities to photoinduced Sb segregation during Raman measurements, although very low laser power (<1 mW) was used in the experiments. Several tests with different laser powers showed important frequency downshifts of Sb modes for as-milled and annealed samples as the laser power increased (up to about 1 mW). These results will be explored and published elsewhere as soon as possible. Another hypothesis is that these lines can be due to other phase(s), neither rhombohedral Sb nor cubic GaSb, indicating a multiphase state. The fitting of the spectrum #2 corroborates the multiphase interpretation, as can be seen in table 1.

(ii) Compared to those for bulk Sb, the low frequency modes are shifted to lower frequency values. Raman measurements performed as a function of hydrostatic pressure have shown negative values of phonon deformation potentials in bulk Sb [28]. Thus, the negative frequency shifts of Sb precipitates in MA samples can be related to compressive stress. The calculated values for the as-milled sample (in the Sb-rich region) were as high as 0.2(1.5) and 1.2(4.4) GPa for E_g and A_{1g} modes, respectively. These are very high pressure values and must induce chemical/structural disorder in the GaSb phase, as suggested by the broadened lines. In the same approach, now considering LO–GaSb mode frequency and pressure induced shifts from [29], the cubic GaSb lattice was estimated to be under tensile stress of about 3.2 GPa. This value combined with the strain obtained from x-ray diffraction furnish moduli of elasticity of 1.06×10^{12} dyn cm^{-2}, which agrees with the reference one for bulk GaSb. The ratio of Sb and GaSb volume coefficients is 1.4 at room temperature. Then one can expect compressive stress on Sb precipitates when the as-milled sample is heated (by the laser spot), while the GaSb nanocrystals tend to be under tensile stress, if we believe that Sb precipitates are in the interface area.

(iii) Similar assumptions can be made for the spectra of the annealed sample, which, according to the XRD fitting pattern, must contain about 5% of Sb. Repeated measurements ensure the reproducibility of the spectra for annealed samples in several different sample positions. In all spectra just very weak A_{1g} and E_g lines with frequencies close to bulk Sb ones (i.e. almost stress free, <0.6 GPa) were observed. Moreover, the cubic GaSb phase remains under tensile stress of about 2.2 GPa. This value and the moduli of elasticity lead to a strain of about 2.0% for the annealed sample and not 0.9% as calculated by means of the x-ray results. Up to now there has been no reasonable answer for this discrepancy.

These results for the low frequency modes of the Raman spectra for the as-milled sample suggest the existence of highly compressed Sb clusters in the interfacial region of tensile GaSb nanocrystals. The fact that they do not corroborate the absence of Sb shown by XRD and DSC measurements for as-milled sample can be understood from the photoinduced Sb segregation caused by local laser heating during Raman measurements or the existence of a new GaSb phase (very similar to the cubic GaSb) that has a Raman profile coincident with those for cubic GaSb and rhombohedral Sb phases. Further x-ray absorption spectroscopy (XANES and EXAFS), Raman and transmission electronic microscopy investigations are being carry out to clarify these interpretations. In addition, recently high pressure Raman measurements on these samples were performed and will be published elsewhere.

4. Conclusions

Nanostructured GaSb alloy was produced by MA starting from two different nominal compositions ($Ga_{50}Sb_{50}$ and $Ga_{30}Sb_{70}$) after being milled for just few hours (9 and 8 h, respectively). Its structural, thermal and optical properties have been investigated and the main conclusions obtained in this study are:

(1) XRD patterns for as-milled and annealed $Ga_{50}Sb_{50}$ samples show the cubic zinc blende GaSb phase nucleation. The annealing only promoted structural relaxation, removing point and line defects, as well as stress and strain, growth of grain size and segregation of the Sb particles. The main difference detected for the $Ga_{30}Sb_{70}$ mixture was the presence of remaining Sb phase.
(2) On the basis of XRD results the exothermic broad bands seen in the DSC curves were attributed to the structural relaxation: elimination of stress, strain, and point and line defects, as well as to the grain growth of the cubic GaSb. The sharp exothermic peak was associated with an amorphous–crystalline (Sb and/or GaSb) phase transformation, although the segregation of the Sb particles cannot be discarded. The melting point of Sb phase was observed just for annealed $Ga_{50}Sb_{50}$ and as-milled $Ga_{30}Sb_{70}$ samples, which corroborates this last possibility.
(3) The mean crystallite size for annealed $Ga_{50}Sb_{50}$ sample is twice that obtained for the as-milled sample.
(4) Raman measurements on as-milled $Ga_{50}Sb_{50}$ samples showed cubic zinc blende GaSb phase and suggested the existence of new GaSb phase in some specific regions. This interpretation is not supported by XRD and DSC results and thus speculations about photoinduced Sb precipitation are inevitable. For the annealed $Ga_{50}Sb_{50}$ sample the GaSb phase and Sb clusters showed similar, but less intense, stress condition scenarios, as suggested for the as-milled sample.

Acknowledgments

The authors wish to thank the Brazilian Agencies FAPESP, CNPq and FINEP for financial support. We are indebted to Dr P B Prates for the XRD measurements.

References

[1] De Lima J C, Trichês D M, dos Santos V H F and Grandi T A 1999 *J. Alloys Compounds* **282** 258
[2] Weeber A W and Bakker H 1988 *Physica* B **115** 93
[3] Mukhopadhyay D K, Suryanarayana C and Froes F H 1994 *Scr. Metall. Mater.* **30** 133
[4] Yavari A R, Desré P J and Benameur T 1992 *Phys. Rev. Lett.* **68** 2235
[5] Gutmanas E Y 1989 *Proc. DGM Conf. on New Materials by Mechanical Alloying Techniques* ed E Arzt and L Schultz (Oberursel: DGM Informationsgesellschaft) p 129
[6] Wang S Q and Ye H Q 2002 *J. Phys.: Condens. Matter* **14** 9579
[7] Wang S Q and Ye H Q 2003 *Phys. Status Solidi* b **240** 45
[8] Pizani P S, Joya M R, Lanciotti F, Jasinevicius R G, Samad R E, de Rossi W, Freitas A Z and Vieira N D Jr 2005 *Proc. 1st Int. Conf. on Diffusion in Solids and Liquids* (Portugal: Aveiro) p 551
[9] Kailer A and Gogotsi K G 1999 *J. Raman Spectrosc.* **30** 939
[10] Pizani P S and Joya M R 2006 *Phys. Rev. Lett.* submitted
[11] Bennett B R, Magno R, Boos J B, Kruppa W and Ancona M G 2005 *Solid State Electron.* **49** 1875
[12] Mourad C, Gianardi D, Malloy K J and Kaspi R 2000 *J. Appl. Phys.* **88** 5543
[13] Hansen M and Anderko K 1991 *Constitution of Binary Alloys* 2nd edn (New York: McGraw-Hill–Genium Publishing Corp.)
[14] Joint Committee on Powder Diffraction Standards (JCPDS) 2000 Philadelphia

[15] Shevchik N J and Paul W 1973/74 *J. Non-Cryst. Solids* **13** 1
[16] Bonefacic A, Tonejc A and Ogorelec Z 1989 *Scr. Metall.* **23** 1121
[17] Ponyatovsky E G and Barkalov O I 1992 *Mater. Sci. Rep.* **8** 147
[18] Sun Y M, Jiang W J and Wu M C 1996 *J. Appl. Phys.* **80** 1731
[19] Tonejc A, Dužević D and Tonejc A M 1991 *Mater. Sci. Eng.* A **134** 1372
[20] Rietveld H M 1969 *J. Appl. Crystallogr.* **2** 65
[21] *TAPP, version 2.2* (Wade Court, Hamilton, OH: E. S. Microwave Inc.)
[22] Williamson G K and Hall W H 1953 *Acta Metall.* **1** 22
[23] Strnad Z 1986 *Glass–Ceramic Materials, Glass Science and Technology* vol 8 (Amsterdam: Elsevier) p 161
[24] Antonov V E, Barkalov O I and Ponyatovsky E G 1995 *J. Non-Cryst. Solids* **192** 443
[25] Inorganic Crystal Structure Database (ICSD) 1995 Gmelin-Institut für Anorganische Chemie and Fachinformationszentrum, FIZ Karlsruhe
[26] Pizani P S and Campos C E M 1998 *J. Appl. Phys.* **84** 6588
[27] Campos C E M and Pizani P S 2001 *J. Appl. Phys.* **89** 3631
[28] Renucci J B 1974 *PhD Thesis* Université Paul Sabatie, Toulouse, France
[29] Trommer R, Anastassakis E and Cardona M 1976 *Light Scattering in Solids* ed M Balkanski, R C Leite and S P S Porto (Paris: Flammarion)